

## Fragment state correlations in the dissociation of NOHF( $v=1$ )

Joanne H. Shorter, Michael P. Casassa, and David S. King

Citation: *The Journal of Chemical Physics* **97**, 1824 (1992); doi: 10.1063/1.463170

View online: <http://dx.doi.org/10.1063/1.463170>

View Table of Contents: <http://scitation.aip.org/content/aip/journal/jcp/97/3?ver=pdfcov>

Published by the [AIP Publishing](#)

---

### Articles you may be interested in

[An analysis of the magnetic hyperfine interactions in the microwave spectrum of NO–HF: Evidence of electron transfer](#)

*J. Chem. Phys.* **115**, 1367 (2001); 10.1063/1.1377027

[A theory for the magnetic hyperfine interactions in the microwave spectrum of NO–HF](#)

*J. Chem. Phys.* **115**, 1355 (2001); 10.1063/1.1377026

[Transition state and dynamics of unimolecular no barrier fragmentation: Thermal dissociation of N<sub>2</sub>O<sub>4</sub>](#)

*J. Chem. Phys.* **105**, 4511 (1996); 10.1063/1.472331

[P-type doubling in the infrared spectrum of NO–HF](#)

*J. Chem. Phys.* **93**, 2992 (1990); 10.1063/1.458886

[Crosscorrelation trajectory study of vibrational relaxation of HF \( \$v=1-7\$ \) by HF \( \$v=0\$ \)](#)

*J. Chem. Phys.* **73**, 4390 (1980); 10.1063/1.440653

---



# Fragment state correlations in the dissociation of NO·HF( $\nu=1$ )

Joanne H. Shorter,<sup>a)</sup> Michael P. Casassa,<sup>b)</sup> and David S. King<sup>b)</sup>

*Molecular Physics Division, National Institute of Standards and Technology,  
Gaithersburg, Maryland 20899*

(Received 29 January 1992; accepted 23 April 1992)

The NO( $\nu, J$ )-fragment population distributions and recoil energies were measured for the vibrational predissociation of NO·HF following excitation of the H–F stretch. Most of the available energy appears in NO vibration and/or HF rotation. There is little recoil momentum. All NO( $\nu, J$ ) fragments are formed with near  $\delta$ -function recoil kinetic energies, correlated with HF fragments in a single rotational level. Two dissociation channels proceed with similar probability to produce NO( $\nu=0$ ) and NO( $\nu=1$ ). Only two rotational levels of HF are populated. One of the HF rotational states is correlated exclusively with NO( $\nu=0$ ) fragments, the other is paired with NO( $\nu=1$ ) fragments. Constraints on fragment angular momenta as well as energetics appear important for the dissociation dynamics. The presence of significant amounts of vibrationally excited NO fragments, in the absence of observable spectroscopic perturbations, implies that intramolecular vibrational redistribution proceeds as the dimer dissociates. The data support two possibilities for the NO·HF dimer bond energy: (1)  $D_0 = 448 \pm 5 \text{ cm}^{-1}$  with coincident pairs of fragments NO( $\nu=0$ ) + HF( $J=12$ ) and NO( $\nu=1$ ) + HF( $J=8$ ); (2)  $D_0 = 1769 \pm 10 \text{ cm}^{-1}$  with  $J_{\text{HF}} = 9$  and 2, respectively.

## I. INTRODUCTION

A strong general effort has been made to investigate the ground-state photodissociation dynamics of weakly bound molecular complexes.<sup>1–4</sup> Closed-shell systems, especially those involving HF,<sup>5–7</sup> have been well studied. Less is known about complexes involving open-shell species, although studies have examined rare-gas complexes with OH,<sup>8,9</sup> and a variety of bimolecular complexes involving NO.<sup>10</sup> The dimers (NO)<sub>2</sub> (Refs. 11 and 12) and (HF)<sub>2</sub> (Refs. 1 and 6) provide interesting points for comparison. They exhibit dramatic differences in their dissociation dynamics that can be traced to characteristic differences in their bonding and fragment energy levels. The HF dimer is prototypical of hydrogen-bonded species, while in the NO dimer the two unpaired electrons share an orbital in a covalent bond. The rotational constant of HF is large, about  $20 \text{ cm}^{-1}$ , while that of NO is much smaller, only  $1.7 \text{ cm}^{-1}$ . In the dissociation of (HF)<sub>2</sub>, nearly all energetically accessible rotational levels of the HF fragments are populated. They are populated in distinct pairs, with interfragment  $J$ – $J$  correlations such that those pairs of fragment rotational levels that minimize recoil energy release are most favored. Conversely, the dissociation of (NO)<sub>2</sub> produces NO fragments in several low- $J$  levels, with no interfragment  $J$ – $J$  correlation and with about 90% of the available energy appearing in fragment recoil.

In this paper the bonding and dissociation dynamics of the mixed NO·HF dimer excited to the  $\nu=1$  level of the H–F stretch are explored using high-resolution Doppler analysis of the resulting NO fragments. Results were obtained for

parent complexes in a narrow range of angular momentum states, predominantly  $K'=0, J'=4.5$ – $6.5$ . Vibrational predissociation of this system is interesting because NO has been shown to be exceptionally effective in the collisional deactivation of HF( $\nu=1$ ),<sup>13</sup> because of its novel bond type, and because energy transfer to the NO( $\nu=1$ ) level is energetically possible during dissociation. These results show the presence of two principal dissociation channels with strong interfragment correlations. Although the NO moiety of the van der Waals dimer is notionally unexcited in the parent, NO fragments are formed in  $\nu=0$  and  $\nu=1$  levels with similar probability. All NO( $\nu, J$ ) fragments are formed with  $\delta$ -function recoil energies. HF( $J$ ) fragments are formed in only two rotational levels. Fragments in one of the levels are associated exclusively with NO( $\nu=0$ ) fragments. Fragments formed in the other level are paired with NO( $\nu=1$ ) fragments. These correlated pairs are formed so as to minimize recoil, resulting in only small amounts of energy being available for NO rotation and spin–orbit excitation. The presence of two competitive vibration–rotation channels is unexpected based on simple theories of collisional vibrational energy transfer and van der Waals vibrational predissociation, which both would favor exclusively the formation of vibrationally excited NO fragments.

The infrared spectrum of the NO·HF( $\nu=1 \leftarrow 0$ ) transition has been recorded using molecular-beam optothermal spectroscopy and analyzed by Fawzy *et al.*<sup>14</sup> The origin of the band is  $3877 \text{ cm}^{-1}$ . This  $84 \text{ cm}^{-1}$  redshift from the HF monomer transition is typical of strong hydrogen bonding. The band has parallel character, with pairs of transitions. The observed  $P$ -type doubling is characteristic of an unpaired-electron spin coupled to the rotational angular momentum of a bent complex with substantially quenched electron orbital angular momentum.<sup>14</sup> Spectral analysis favors an equilibrium geometry with the HF axis aligned with the

<sup>a)</sup> NIST National Research Council Postdoctoral Fellow 1990–91. Permanent address: Aerodyne Research Inc., 45 Manning Rd., Billerica, MA 01821.

<sup>b)</sup> Physics Laboratory, Technology Administration, U.S. Department of Commerce.

H atom pointing toward the NO center of mass, a centers-of-mass bond distance of 3.4 Å, and an NO–HF angle of  $30 \pm 15^\circ$ . Transitions originating from NO·HF levels with  $K=0$  and  $J=0-5$  exhibited uniform, homogeneously broadened widths corresponding to predissociation lifetimes of about 0.8 ns.

## II. EXPERIMENT

The NO·HF dimer was produced in a pulsed supersonic expansion<sup>11</sup> of a mixture of NO and HF in Ar through a 0.75 mm diam nozzle. Both reactants were vacuum distilled prior to use. Usable NO·HF dimer yield accompanied by a low beam temperature was obtained with mole fractions of NO and HF of about 2% and 1.5%, respectively. Backing pressures of  $1.6 \times 10^5$  and  $4.3 \times 10^5$  Pa [25 and 65 psi (absolute)] were used, and gave essentially identical results. The pulsed-pump and pulsed-probe lasers crossed the free-jet expansion about 15 nozzle diameters downstream from the nozzle orifice. This is a region where there are no collisions within the 10 ns time delay between excitation and probing pulses.

Infrared (IR) pump pulses at 2.3  $\mu\text{m}$  to excite the H–F stretching fundamental of the complex were obtained by nonlinear optical techniques.<sup>15,16</sup> The difference frequency between the 670 nm output of a YAG-pumped dye laser and the 532 nm YAG second harmonic was generated in LiIO<sub>3</sub> (YAG denotes yttrium aluminum garnet). The low-energy output of this difference frequency generator was amplified parametrically in a pair of LiNbO<sub>3</sub> crystals, pumped by 1064 nm YAG fundamental. The YAG laser used in these experiments was a single-mode, injection-seeded system, with a transform limited output at 1064 nm of nominally 7 ns duration and  $0.002 \text{ cm}^{-1}$  bandwidth. The net IR output was about 250  $\mu\text{J}$  in a  $0.3 \text{ cm}^{-1}$  bandwidth in the region of 3880  $\text{cm}^{-1}$ . The IR beam was focused into the photolysis chamber, producing a beam waist of 0.3 mm in the photolysis region. The entire IR beam path was enclosed and flushed with dry nitrogen to eliminate atmospheric absorption. The absolute IR wavelength was calibrated by comparison to the published NO·HF dimer spectrum<sup>14</sup> and reference water absorptions.<sup>17</sup>

The results emphasized here were obtained with the IR pump tuned to 3878.5  $\text{cm}^{-1}$ . Although the  $0.3 \text{ cm}^{-1}$  bandwidth did not allow excitation of individual dimer transitions, this principally excites  $K=0$  dimers on the  $R(3.5)$  to  $R(5.5)$  transitions, exciting both  $P$ -doublet species. Under these conditions the vibrationally excited parents have internal energies within the range  $3880.4 \leq E_{\text{parent}} (\text{cm}^{-1}) < 3883.2$ . Photodissociation action spectra, recorded scanning the IR pump wavelength while monitoring ultraviolet (UV) NO-fragment laser-induced fluorescence (LIF), and band-contour simulations<sup>18</sup> indicate a rotational temperature of about 10 K, dependent on expansion conditions. Given the nominal 10 K temperature of the expansion, there is a small component of  $K=1$  species which are excited at this wavelength. The continuous expansion used by Fawzy *et al.* to obtain and analyze the NO·HF( $v=1 \leftarrow 0$ ) spectrum<sup>14</sup> resulted in a dimer rotational temperature of 2 K, in which there was not a sufficient  $K>0$  population for spectroscopic

analysis. These  $K=1$  species carry an approximate additional  $10 \text{ cm}^{-1}$  of internal energy<sup>14</sup> and their relative population is sensitive to expansion conditions.

The NO fragments were probed by single-photon LIF.<sup>11</sup> Narrow-band pulses at 226 nm were generated by pulse amplification of the continuous-wave output of a narrow-band, ring laser. This was followed by second-harmonic generation and sum frequency mixing with narrow-band 1064 nm YAG fundamental. The resulting UV pulses had bandwidths of ca. 140 MHz. Both collinear and orthogonal pump-probe geometries were used.<sup>19,20</sup> In the collinear geometry a collimated 200  $\mu\text{m}$  diam probe beam of 0.01  $\mu\text{J}$  energy was used; in the orthogonal configuration, 1–2  $\mu\text{J}$  of 226 nm output was loosely focused with a cylindrical lens to a line of dimension 10 mm by 0.2 mm. Control measurements were taken to ensure the LIF signals under these conditions were linear with probe-laser energy, and that the measured Doppler profiles were independent of probe-laser energy.

For many of the fragment levels populated by dissociation, there was also an IR-pump laser-independent signal from the beam-cooled NO monomer. Therefore each Doppler profile measurement consisted of the recording of pairs of probe-laser frequency scans, with and without the pump laser present. During each scan of the ring laser frequency, the fragment LIF signal intensity, probe-laser energy, and pump-laser energy were recorded, indexed to the frequency of the ring laser at 25 MHz (visible) step intervals. For each of these scans the LIF signal was first point-by-point normalized to the UV probe-laser pulse energy. Second, the background scan, which includes information on the beam-cooled monomer (probe-laser frequency dependent) and laser scatter (independent of laser frequency) was fit to a Gaussian line profile, characterized by a full width at half maximum (FWHM) and a zero offset. A Gaussian profile is anticipated for the residual Doppler motion in the unskimmed expansion. As an example, expansion-cooled  $^2\Pi_{1/2}$  NO( $v=0, J=1.5$ ) exhibited a 700 MHz FWHM Gaussian line profile, corresponding to a 15 K translational temperature. The fitted Gaussian line profiles of the background exhibited 600–800 MHz FWHM, slightly dependent on  $J$ . Smooth, best-fit “background” curves were then subtracted from the signal. For all the data discussed here, the background contribution was less than 10% of the total signal. Finally, the resulting photodissociation signal was normalized point by point to IR pump-laser energy.

The NO( $A \leftarrow X$ ) transitions<sup>21</sup> used in this study to probe  $^2\Pi_{1/2}$  NO( $v, J$ ) species were the  $S_{21}$  lines of the (0,0) and (1,1) vibronic bands; for  $^2\Pi_{3/2}$  NO( $v, J$ ) species the  $O_{12}$  lines were used. Transitions such as those generally referred to as “ $Q_{11}$ ” lines are actually near blends of transitions from the same ground-state level to a pair of spin-rotation split levels in the upper state. These two upper-state, spin-rotation levels are separated in energy by a small amount, and are normally considered degenerate. However, since the recoil energies released in the present experiments are so low, the few hundred MHz excited-state, spin-rotation splittings are readily noticeable and contribute significant width to the observed line profiles.

### III. RESULTS AND DISCUSSION

Typically, 6–10 Doppler profiles for each fragment state and geometry were summed, fit to the expression

$$g(\nu) = (2\Delta\nu_D)^{-1} [1 + \beta_{\text{eff}} P_2((\nu - \nu_0)/\Delta\nu_D)], \quad (1)$$

and convoluted with a Gaussian experimental resolution function,  $\Delta\nu_G$ . This represents the Doppler profile for molecules with a  $\delta$ -function speed distribution and with an effective anisotropy  $\beta_{\text{eff}}$  that accounts for flux anisotropy and other vector correlations. If NO fragments in each specific quantum state all had HF cofragments in a single quantum state, by conservation of energy they would have  $\delta$ -function recoil kinetic-energy distributions. The single recoil speed results in a maximum Doppler shift of  $\pm \Delta\nu_D$  about the transition rest frequency  $\nu_0$ . In these experiments, the resolution limiting factor was not the ca. 140 MHz bandwidth of the probing laser, but the transverse spread of parent-dimer motion in the photolysis zone. This arises even if the dissociation process were to impart a  $\delta$ -function speed distribution to the NO( $\nu, J$ ) fragments, since the final velocity distribution of these fragments will include the spread of initial parent motions. In our experimental geometry, the important parent motion is that transverse to the flow stream of the molecular beam and parallel to the propagation direction of the probe laser. Characterization of line profiles for low- $J$ , beam-cooled monomers provides a value  $\Delta\nu_G = 700$  MHz FWHM. Analysis of the fragment Doppler line shapes gives information on the recoil energetics discussed in Sec. III A. Integration of these Doppler profiles results in relative rovibrational populations discussed in Sec. III B.

#### A. Recoil

Two resulting Doppler profiles and fits are presented in Fig. 1. These are for  ${}^2\Pi_{3/2}$  NO( $\nu=0, J$ ) fragments in rotational levels  $J=2.5$  (trace A) and  $8.5$  (trace B), with internal energies of 133 and 257  $\text{cm}^{-1}$ , respectively. One trend illustrated by these two profiles is that fragments in higher-energy states have lower recoil energies, i.e., narrower Doppler profiles. The observed widths of these two profiles are nominally 1900 and 850 MHz FWHM, respectively. For all of the levels probed, the observed Doppler widths were not more than a factor of 3 greater than the 700 MHz FWHM resolution function. As shown below,  $\beta_{\text{eff}} \approx 0$ . This should result in a square-wave Doppler profile. All the curvature of the sloping edges of the observed profiles is due to the effects of  $\Delta\nu_G$ , the initial parent-dimer motion. This translates into a situation where fitting the observed spectra to Eq. (1) does not result in unique solutions for the variables  $\beta_{\text{eff}}$ ,  $\Delta\nu_D$ , and  $\Delta\nu_G$ . For example, in analyzing the data in Fig. 1(B), equally good fits were obtained for pairs of values  $\beta_{\text{eff}} = 0.2$  and  $\Delta\nu_D = 370$  MHz,  $\beta_{\text{eff}} = 0.0$  and  $\Delta\nu_D = 420$  MHz, and  $\beta_{\text{eff}} = -0.2$  and  $\Delta\nu_D = 440$  MHz, all with a value of  $\Delta\nu_G = 700$  MHz FWHM. If overlaid on Fig. 1(B), fits for these different parameters would differ by little more than the thickness of the drawn fit line. Although this does not allow unique determinations of these fitting parameters, the total recoil energy determined only varies from 21 to 30  $\text{cm}^{-1}$ , so that there is a good determination of

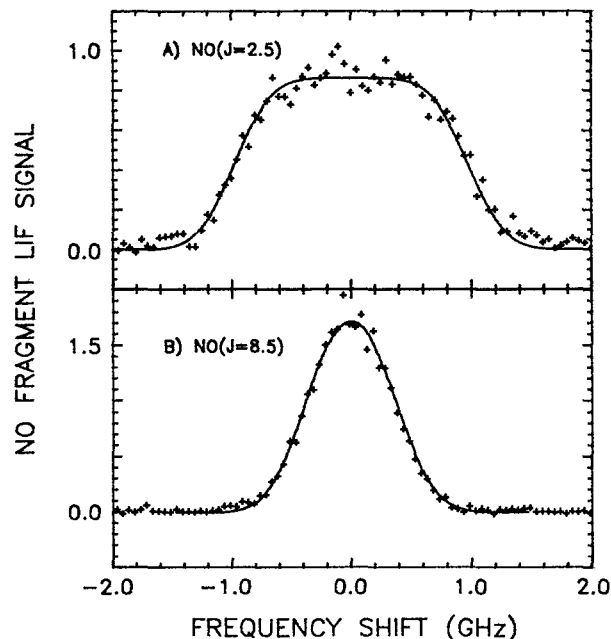


FIG. 1. Doppler profiles (+) for  $O_2^0(J)$  transitions probing  ${}^2\Pi_{3/2}$  NO( $\nu=0, J$ ) fragments for (A)  $J=2.5$  and (B)  $J=8.5$ , and fits (solid lines) to single  $\delta$ -function speed distributions as discussed in the text.

this feature of the dynamics. For consistency, all the measured profiles were initially fit with the value of  $\beta_{\text{eff}}$  set at zero and the Gaussian resolution function fixed at  $\Delta\nu_G = 700$  MHz FWHM. Fitting these Doppler profiles results in the determination of a single recoil speed, which in turn determines the recoil energy of the NO( $\nu, J$ )-fragment level probed and (from conservation of linear momentum) of its HF cofragment. For a number of averaged profiles, fits were performed for varied values of  $\Delta\nu_G$  and  $\beta_{\text{eff}}$  to obtain allowable ranges for these parameters and to determine the sensitivity of the derived recoil energies to them. The effects on derived recoil energy of fixing these fitting parameters at  $\beta_{\text{eff}} = 0$  and  $\Delta\nu_G = 700$  MHz are small and will be discussed below, along with the range of acceptable values for  $\beta_{\text{eff}}$  and  $\Delta\nu_G$ .

The data are all fit well by the assumed single  $\delta$ -function speed distributions, as illustrated in Fig. 1. That other distributions are unacceptable is shown graphically in Fig. 2, where the Doppler profile for  ${}^2\Pi_{3/2}$  NO( $\nu=0, J=8.5$ ) fragments is shown again, with a fitted curve calculated assuming that 85% of the cofragments were HF( $J=9$ ) and 15% HF( $J=8$ ) (the fit in Fig. 1 assumes 100% of the HF-cofragment population to be in a single level.) The broad wings in the simulation arise from NO fragments formed coincident with HF( $J=8$ ) species, and are significantly different from the data. Not only is the fitting in the wings poor, but adding in contributions to the Doppler simulation from NO molecules formed in coincidence with HF( $J=8$ ) cofragments also results in the failure to fit the peak of the observed Doppler profile. The determined recoil energy for this NO fragment, 23  $\text{cm}^{-1}$ , is so low that higher-energy rotational levels of the HF cofragment, i.e., HF( $J \geq 10$ ) are

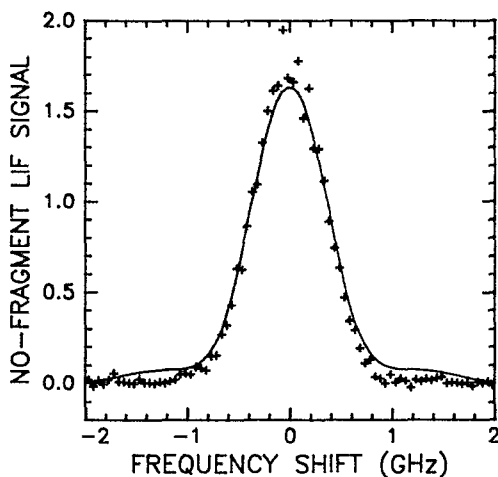


FIG. 2. Doppler profile (+) for the  $O_{12}^{00}(8.5)$  transition probing  ${}^2\Pi_{3/2}$  NO( $\nu=0, J=8.5$ ) fragments, and fit (solid line) assuming HF cofragments in two rotational levels as discussed in text.

energetically closed. There is not sufficient structure or width in this Doppler profile to support any significant HF-cofragment population in more than a single rotational level. This is true for all NO( $\nu, J$ )-fragment transitions observed. The experimental signal to noise places an upper limit of about 5% on the relative HF-cofragment population allowed in other rotational levels.

Figure 3(A) plots the total recoil energy,  $E_{\text{recoil}}$ , obtained from the Doppler analysis, against  $E_{\text{internal}}^{\text{NO}(\nu=0)}$  for each NO( $\nu=0, J$ ) level probed. The triangles and circles represent data obtained for NO( $\nu=0, J$ ) fragments formed in the  ${}^2\Pi_{1/2}$  and  ${}^2\Pi_{3/2}$  spin-orbit states, respectively. Data are not presented for levels with internal energies less than ca. 130  $\text{cm}^{-1}$ , due to large beam-cooled monomer contributions for these levels. The solid line is the best linear fit to the data forced to have a slope of  $-1$ . This situation is required by conservation of energy if all NO( $\nu=0, J$ ) fragments have HF( $J_0$ ) cofragments in the same  $J_0$  rotational state. The  $E_{\text{recoil}}^{\text{NO}(\nu=0)} = 0 \text{ cm}^{-1}$  intercept for the data shown in Fig. 3(A) gives directly the amount of energy available,  $E_{\text{available}}^{\text{NO}(\nu=0)}$ , for internal excitation of NO,  $E_{\text{internal}}^{\text{NO}(\nu=0)}$ , and fragment recoil in conjunction with the formation of HF( $J_0$ ) fragments with rotational energy  $E_{\text{rotation}}^{\text{HF}(J_0)}$ . The data presented in Fig. 3(A) gives the value  $E_{\text{available}}^{\text{NO}(\nu=0)} = 280 \pm 10 \text{ cm}^{-1}$ .

There is a significant probability of forming NO( $\nu=1$ ) fragments. These NO( $\nu=1$ ) fragments are only formed in very low rotational levels of the  ${}^2\Pi_{1/2}$  spin-orbit state. No fragment population was observed in  ${}^2\Pi_{3/2}$  NO( $\nu=1, J$ ) levels. As discussed for the NO( $\nu=0, J$ ) fragments, the NO( $\nu=1, J$ ) fragments can be shown to have HF( $J_1$ ) cofragments in a single rotational level. Recoil energies for the  ${}^2\Pi_{1/2}$  NO( $\nu=1, J$ ) fragments are presented in Fig. 3(B), determined as above except that there was negligible beam-cooled background for all but the NO( $\nu=1, J=0.5$ )-fragment level, which is not included. The best-fit line of slope  $-1$  has an  $E_{\text{recoil}}^{\text{NO}(\nu=1)} = 0 \text{ cm}^{-1}$  intercept that gives

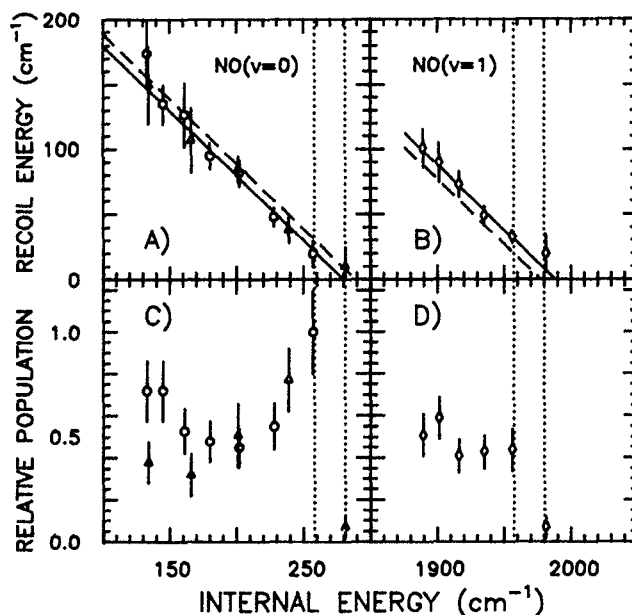


FIG. 3. Recoil energies measured (A) ( $\Delta$ ) for  ${}^2\Pi_{1/2}$  NO( $\nu=0, J$ ) fragments and (O) for  ${}^2\Pi_{3/2}$  NO( $\nu=0, J$ ) fragments; and (B) ( $\diamond$ ) for  ${}^2\Pi_{1/2}$  NO( $\nu=1, J$ ) fragments. Relative rotational populations (C) ( $\Delta$ ) for  ${}^2\Pi_{1/2}$  NO( $\nu=0, J$ ) fragments and (O) for  ${}^2\Pi_{3/2}$  NO( $\nu=0, J$ ) fragments; and (D) ( $\diamond$ ) for  ${}^2\Pi_{1/2}$  NO( $\nu=1, J$ ) fragments plotted against NO( $\nu, J$ )-fragment internal energy. Note the x-axis scale breaks between the NO( $\nu=0$ ) and NO( $\nu=1$ ) data.

$$E_{\text{available}}^{\text{NO}(\nu=1)} = 1988 \pm 5 \text{ cm}^{-1} [E_{\text{vib}} = 1876 \text{ cm}^{-1} + E_{\text{rot}} = 112 \pm 5 \text{ cm}^{-1} (\pm 1\sigma \text{ error based on statistical uncertainties})].$$

Doppler profiles were measured in the orthogonal pump-probe geometries<sup>16,20</sup> IV and VI to assess the extent of  $\mu\nu$  and  $\nu\mathbf{J}$  vector correlations in the dissociation process ( $\mu$  being defined in terms of the parent transition dipole moment and  $\nu, \mathbf{J}$  the fragment velocity and angular momentum vectors, respectively). The Doppler profiles obtained in each of these geometries were essentially identical. A weighted sum of profiles,  $2 \cdot \text{IV} + \text{VI}$  gives a composite profile for which the only source of anisotropy arises from  $\nu\mathbf{J}$  correlation. Such a composite profile for  ${}^2\Pi_{3/2}$  NO( $\nu=0, J=3.5$ ) fragments is shown in Fig. 4 by the + symbol. In fitting this composite profile to Eq. (1),  $\beta_{\text{eff}} = b_3 \beta_{\nu\mathbf{J}}$ . The bipolar multiplier for the  $O_{12}^{00}(3.5)$  transition used is  $b_3 = .53$ . Although best fit by  $\beta_{\nu\mathbf{J}} = 0$ , acceptable fits were obtained for values of  $-0.5 < \beta_{\nu\mathbf{J}} < 0.5$  ( $\beta_{\nu\mathbf{J}}$  can have values in the range  $-0.5$  to 1;  $\beta_{\nu\mathbf{J}} = -0.5$  corresponds to  $\mathbf{J}$  orthogonal to  $\nu$ ). The fit to this data in Fig. 4 is for  $\beta_{\nu\mathbf{J}} = 0$ . The difference between profiles, i.e., IV-VI, is sensitive to  $\beta_{\mu\nu}$ , emphasizing the extent of  $\mu\nu$  correlation. Such a difference for the  $O_{12}^{00}(3.5)$  transition is presented in Fig. 4 by dots. Fitting of this "residual" indicates  $|\beta_{\mu\nu}| < 0.1$ . The fit to this second composite profile included in this figure is for  $\beta_{\mu\nu} = 0.05$ .

The error bars imposed in Figs. 3(A) and 3(B) and the above-mentioned values of  $E_{\text{available}}^{\text{NO}(\nu)}$  represent ( $1\sigma$ ) statistical uncertainties arising from the limited experimental signal to noise and the sensitivity of fitting  $\Delta\nu_D$  to the Doppler data for each fragment level. Additionally, there are two

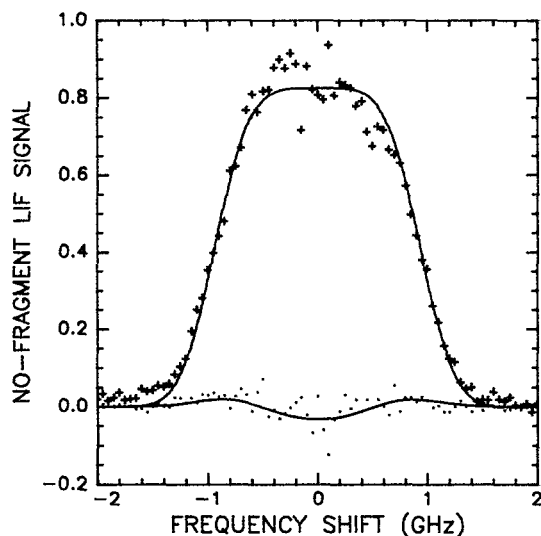


FIG. 4. Composite Doppler profiles for the  $O_{12}^{00}(3.5)$  transition probing  ${}^2\Pi_{3/2}$  NO( $\nu=0, J=3.5$ ) fragments: (+) adding twice the averaged profile obtained in geometry IV plus that in geometry VI to emphasize  $\nu J$  correlations; (o) the difference between profiles obtained in IV-VI to emphasize  $\mu\nu$  correlation. The solid lines are fits discussed in the text.

sources of systematic error in determining recoil energies that have not been included in the error bars in Fig. 3. First, the experimental resolution function  $\Delta\nu_G = 700$  MHz FWHM was fixed in the fitting to represent the spread of initial motions of the parent dimers. This is the best-fit number for this contribution and is consistent with measured line profiles for the low- $J$  beam-cooled NO monomer and with results in earlier vibrational predissociation experiments.<sup>11</sup> Qualitatively good fits to the observed Doppler profiles were, however, obtained for values in the range 500–800 MHz. The result of having fixed  $\Delta\nu_G$  at 700 MHz introduces a possible systematic error of up to  $\pm 4$   $\text{cm}^{-1}$  into the determined recoil energies. Second, all fits were made fixing  $\beta_{\text{eff}} = 0$ . Acceptable fits were obtained with values for  $\beta_{\text{eff}}$  in the range  $-0.5 < \beta_{\text{eff}} < 0.2$ , with concomitant changes in the fitted Doppler shifts. This introduces possible systematic errors of up to  $\pm 6$   $\text{cm}^{-1}$  to the extracted recoil energies. The net result of these two potential sources of systematic error would be to uniformly shift the derived recoil energies by up to  $\pm 10$   $\text{cm}^{-1}$  ( $1\sigma$ ); correspondingly changing the determined  $E_{\text{available}}^{\text{NO}(\nu)}$  by the same amount. The potential error contribution from assuming  $\Delta\nu_G = 700$   $\text{cm}^{-1}$  will be the same for all reaction channels proceeding from the same parent species. If the vector correlations for both reaction channels are the same, an assumption we make but cannot prove, then this contribution to systematic error will also be the same for both channels. Therefore, the corrections to the determined recoil energies from systematic errors will not influence the difference in  $E_{\text{available}}^{\text{NO}(\nu)}$  for these two channels.

## B. Rovibrational populations

The relative populations of the NO fragment states probed are presented in Figs. 3(C) and 3(D). Surprisingly,

NO( $\nu=0, J$ ) and NO( $\nu=1, J$ ) fragments are formed with similar probability. The NO( $\nu=0, J$ ) fragment rotational state distributions for both spin-orbit states are marked by populations that increase with internal energies up to an energetic cutoff around  $E_{\text{internal}}^{\text{NO}(\nu=0)} \approx 275$   $\text{cm}^{-1}$ , with negligible population at levels of higher energy. The levels of maximum probability are  ${}^2\Pi_{1/2}$  NO( $\nu=0, J=11.5$ ) and  ${}^2\Pi_{3/2}$  NO( $\nu=0, J=8.5$ ). The slight population in the next-higher-energy level  ${}^2\Pi_{1/2}$  NO( $\nu=0, J=12.5$ ) was sensitive to expansion conditions, probably resulting from excitation and dissociation of higher energy,  $K > 0$  parent dimer. Since  $J_{\text{max}}$  is different for the two spin-orbit states, the sharp declines observed in the NO( $\nu=0, J$ ) population distributions above levels for which  $E_{\text{internal}}^{\text{NO}(\nu=0)} \approx 275$   $\text{cm}^{-1}$  cannot be due to simple angular momentum constraints, but arise from conservation of energy. If the dimer bond energy were 450  $\text{cm}^{-1}$  (see below), then the dissociation to form HF( $J=11$ ) +  ${}^2\Pi_{3/2}$  NO( $\nu=0, J=18.5$ ) would be nearly resonant. Attempts were made to probe populations in  ${}^2\Pi_{3/2}$  NO( $\nu=0, J$ ) levels with values of  $J$  between 9.5 up to 19.5, with null results. The absence of NO-fragment population in this level supports an overall picture, however, of the dissociation dynamics being dependent on both energy and angular momentum considerations.

It was not possible to determine the populations in the  ${}^2\Pi_{3/2}$  NO( $\nu=0, J=1.5$ ) level or in the levels  ${}^2\Pi_{1/2}$  NO( $\nu=0, J \leq 7.5$ ) due to large background contributions from the beam-cooled monomer. Therefore it is not possible to determine the spin-orbit branching ratio for NO( $\nu=0$ ) fragments. In the energy region  $150 < E_{\text{internal}}^{\text{NO}(\nu=0)}$  ( $\text{cm}^{-1}$ )  $< 275$ , however, there is essentially no preference for populating either spin-orbit state.

It also is not possible to give a precise measure for the NO( $\nu=1$ )/NO( $\nu=0$ ) population ratio since it was not possible to determine relative populations in the low- $J$ , NO( $\nu=0$ ) levels. The individual NO( $\nu, J$ ) populations are, however, similar. The relative scaling of the NO( $\nu=0, J$ ) to NO( $\nu=1, J$ ) populations in Fig. 3, which is dependent on the observed LIF signal intensities, Franck-Condon factors, and the wavelength dependence of the fluorescence detection system, was obtained by comparison to earlier results on the overtone dissociation of NO dimer for which the NO( $\nu=1$ ) to NO( $\nu=0$ ) ratio is known.<sup>11</sup> The precision in the relative populations NO( $\nu=0$ ) and NO( $\nu=1$ ) is  $\pm 30\%$ .

For NO( $\nu=1, J$ ) fragments there is a sharp decrease in population above  $E_{\text{rotation}}^{\text{NO}(\nu=1)} \approx 100$   $\text{cm}^{-1}$  ( $E_{\text{internal}}^{\text{NO}(\nu=1)} \approx 1976$   $\text{cm}^{-1}$ ). The small population in the  ${}^2\Pi_{1/2}$  NO( $\nu=1, J=7.5$ ) level was sensitive to expansion conditions, and there was no measurable population in higher levels. No  ${}^2\Pi_{3/2}$  NO( $\nu=1, J$ ) fragments were observed, although attempts were made to probe levels with  $1.5 < J < 12.5$ . These levels all have  $E_{\text{internal}} > 2000$   $\text{cm}^{-1}$ , and are not energetically open in the near-resonant dissociation channel that populates the observed  ${}^2\Pi_{1/2}$  NO( $\nu=1, J$ ) levels. The NO( $\nu=1, J$ ) rotational population distribution is fairly flat, perhaps peaked at levels of lowest angular momenta. There is no enhancement of population in the essen-

tially resonant  ${}^2\Pi_{1/2}$  NO( $v=1, J=6.5$ ) final state. This is contrary to the population distribution observed for NO( $v=0, J$ ), which favored those final states which minimized recoil momentum, and suggests that angular momentum constraints play a more important role in the dissociation dynamics of this latter reaction channel.

Collisional vibrational energy transfer for HF( $v=1, 2$ ) has been extensively studied.<sup>13</sup> Relaxation rates have been measured for many colliders, and shown to scale consistently with the vibrational,  $V \rightarrow V$  energy gap. Although the data for these colliders appears to fall into two groups, homonuclear diatomics vs heteronuclear diatomics and polyatomics, the relaxation probability for both groups declines about 1 order of magnitude for every  $600 \text{ cm}^{-1}$  increase in energy gap. Therefore, for molecular colliders with vibrational level structures that provide for near-resonant *intermolecular*  $V \rightarrow V$  transfer, the  $V \rightarrow V$  channel has always been claimed to provide the dominant contribution to the relaxation process. Although the rate for HF( $v=1$ ) relaxation by CO, which has nearly the same rotational constant and dipole moment as NO, is consistent with the energy-gap picture obtained for the other colliders studied, relaxation by NO is an order of magnitude faster than anticipated based on this energy gap. This significant enhancement in vibrational energy transfer for NO has been attributed to an increased attractive interaction between HF( $v=1$ ) and the NO radical.<sup>13</sup> Explicit in the collisional vibrational energy-transfer discussion is the assumption that only the  $V \rightarrow VR$  channel should be active, while the probability of the strictly  $V \rightarrow RT$  channel would be down by a factor of  $10^3$  based on its larger energy gap. The vibrational predissociation of NO·HF( $v=1$ ) is remarkable because near-resonant  $V \rightarrow R$  and  $V \rightarrow VR$  processes have similar probability. This is consistent with the energy-gap model, so successfully applied to collisional vibrational energy transfer, since the recoil energies available through both these processes are so similar and so low. However, the observation of competitive,  $V \rightarrow VR$  and  $V \rightarrow R$  channels requires reevaluation of common assumptions about vibrational energy transfer and suggests the need to revisit the collisional relaxation studies with double-resonance experiments to identify the active channels.

There are several weakly bound systems involving HF that dissociate following vibrational excitation to produce fragments with little recoil energy, consistent with energy- and momentum-gap laws.<sup>1</sup> There is, however, only one case of vibrational predissociation for which a near  $\delta$ -function rotational population distribution has been observed.<sup>9</sup> This was for a rare-gas-diatom system, for which the internal structure of the Ne cofragment is not important. Dissociation of Ne·OH( $v=1$ ) produced principally OH( $N=12$ ) fragments, while Ne·OD( $v=1$ ) dissociated to produce OD( $N=15$ ). These are the reaction channels that minimize recoil. The  $V \rightarrow R$  dissociation through these rotational resonances was slow, exhibiting a  $3 \mu\text{s}$  dissociation lifetime. Experiments on Ar·OH, for which the interaction potential is somewhat stiffer, have shown the OH( $N$ ) fragments to be formed in a range of rotational levels, giving a "cold" rotational population distribution. This pseudo  $V \rightarrow T$  type relaxation goes at a rate  $10^5$  times faster than the Ne·OH dissocia-

tion, with a 30 ps lifetime.

Spectroscopic studies of several van der Waals species<sup>22-24</sup> have indicated dramatic increases in dissociation rates (i.e., broadening of linewidths) when localized intermolecular  $V \rightarrow VR$  resonances are possible. For example, consider the isotopic dependence of the vibrational predissociation of  $\text{D}_2 \cdot \text{HF}(v=1)$  vs  $\text{H}_2 \cdot \text{HF}(v=1)$ .<sup>24</sup> For  $\text{D}_2 \cdot \text{HF}(v=1)$ , the  $\text{D}_2(v=1)$  fragment channel is open and lowers the vibrational energy gap substantially. This system dissociates with a predissociation lifetime of 1.2 ns, which is comparable to the 0.8 ns NO·HF( $v=1$ ) lifetime.<sup>14</sup> For  $\text{H}_2 \cdot \text{HF}(v=1)$ , the  $\text{H}_2(v=1)$  channel is energetically closed. This dissociation must proceed via a  $V \rightarrow R$  type process and does so at a rate about 20 times slower than that of the  $\text{D}_2 \cdot \text{HF}(v=1)$   $V \rightarrow V$  process. The dominance of a single  $V \rightarrow V$  channel has been favored in most theoretical treatments of van der Waals vibrational predissociation,<sup>25</sup> as in discussions of collision-induced vibrational energy transfer.<sup>13</sup> That vibrational excitation migrates across the weak van der Waals bond in the  $\text{D}_2 \cdot \text{HF}(v=1)$  and NO·HF( $v=1$ ) dissociations, although an interesting observation, is anticipated based on momentum-gap arguments and analogy to collisional energy-transfer results. Although their dissociation lifetimes are essentially equal and a single  $V \rightarrow V$  dissociation channel has been proposed<sup>24,25</sup> for  $\text{D}_2 \cdot \text{HF}(v=1)$ , the presence of competing  $V \rightarrow V$  and  $V \rightarrow R$  channels have been demonstrated herein for NO·HF( $v=1$ ).

The unexpected observation of two vibrationally distinct dissociation channels proceeding at similar rates suggests that an anharmonic resonance involving the low-frequency van der Waals modes might be operating.<sup>26</sup> Ideas of this sort have been developed by Ewing to explain the rich vibrational dynamics exhibited in electronically excited Ar-tetrazine clusters, for which strong  $V \rightarrow V$  propensities, dependent on initial vibronic excitation, are observed. In terms of quantum numbers designating  $v_{\text{HF}}$ ,  $v_{\text{NO}}$ ,  $J_{\text{HF}}$ ,  $J_{\text{NO}}$ , and the van der Waals stretch, the simplest picture has the zero-order state  $|1,0,0,0,0\rangle$  coupled independently to two continua built upon  $|0,0,m,n,q\rangle$  and  $|0,1,m',n',q'\rangle$ . Relative rates may be estimated using a propensity formula given by Ewing, wherein the rate is determined by the sum of quantum number changes in each coordinate:

$$\tau^{-1} \approx 10^{13} \exp[-\pi(\Delta n_t + \Delta n_r + \Delta n_v)].$$

To determine the quantum number change in the translational (van der Waals stretching) coordinate, we use Ewing's formulas and Morse potential parameters based on the  $450 \text{ cm}^{-1}$  bond energy and  $3.4 \text{ \AA}$  centers-of-mass separation. We find  $\Delta n_t + \Delta n_r + \Delta n_v \approx 25$  for the most efficient NO( $v=0$ ) path,  $|0,0,12,8.5,3\rangle$ . Similarly,  $\Delta n_t + \Delta n_r + \Delta n_v \approx 15$  for the most efficient NO( $v=1$ ) path,  $|0,1,8,1.5,5\rangle$ . This large difference in quantum number changes makes comparable probabilities for the two paths seem unlikely. Alternatives to this zero-order picture have the chemical motions mixed in the equilibrium geometry, i.e., during excitation, or at internuclear separations and angles experienced during dissociation. However, the observed

NO·HF( $v=1$ ) spectrum showed no evidence of perturbations from an anharmonic resonance.<sup>14</sup> This favors a picture of substantial intramolecular energy flow from the notionally excited HF stretch to the unexcited NO stretch during the dissociation event.

### C. Interfragment correlations

We distinguish between the two channels resulting in NO( $v=0$ ) and NO( $v=1$ ) fragments since these have distinct HF cofragments and energetics:

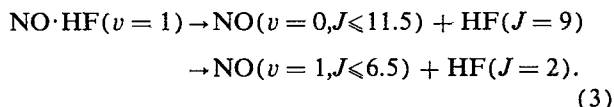
$$E_{\text{available}}^{\text{NO}(v=0)} = E_{\text{parent}} - D_0 - E_{\text{rotation}}^{\text{HF}(J_0)}, \quad (2a)$$

$$E_{\text{available}}^{\text{NO}(v=1)} = E_{\text{parent}} - D_0 - E_{\text{rotation}}^{\text{HF}(J_1)}, \quad (2b)$$

where the internal energy of the excited parent dimers is  $E_{\text{parent}} = 3881.8 \pm 1.4 \text{ cm}^{-1}$ . If the dimer bond energy  $D_0$  were known, the identity of  $J_i$  would be known; conversely, if either  $J_i$  could be identified, then the bond energy is determined very accurately. The difference in  $E_{\text{recoil}} = 0 \text{ cm}^{-1}$  intercepts for these two channels is just equal to the difference in rotational energy in the two corresponding HF fragments:

$$\Delta E_{\text{available}} = E_{\text{rotation}}^{\text{HF}(J_0)} - E_{\text{rotation}}^{\text{HF}(J_1)} = 1708 \pm 12 \text{ cm}^{-1} (1\sigma).$$

This experimental value is close to the energy difference of  $1710 \text{ cm}^{-1}$  for HF species<sup>27</sup> in rotational levels with  $J_0 = 9$  and  $J_1 = 2$ . This suggests two principal reaction channels proceeding with similar probability:



Equations (2) and (3) then give a dimer bond energy of approximately  $1775 \text{ cm}^{-1}$ . The bond energy and interfragment  $J$ - $J$  correlations impose energetic limits on possible values of  $E_{\text{recoil}}$  and on  $E_{\text{internal}}^{\text{NO}(v)}$ . One small inconsistency with a  $1775 \text{ cm}^{-1}$  bond energy is the experimental failure to observe significant population in the  ${}^2\Pi_{1/2}$  NO( $v=1, J=7.5$ ) level, for which  $E_{\text{internal}}^{\text{NO}(v=1)} = 1981 \text{ cm}^{-1}$  and which should be energetically open. Allowing, as would be justified if  $\Delta\nu_G$  were larger than  $700 \text{ MHz}$  and  $\beta_{\text{eff}}$  were positive, for the presence of an  $8 \text{ cm}^{-1}$  systematic error in the determined recoil energies results in values of  $E_{\text{available}}^{\text{NO}(v=0)} = 272 \pm 10 \text{ cm}^{-1}$  and  $E_{\text{available}}^{\text{NO}(v=1)} = 1980 \pm 10 \text{ cm}^{-1}$ , in the  ${}^2\Pi_{1/2}$  NO( $v=1, J=7.5$ ) level being energetically closed (consistent with observation), and in a value of  $D_0 = 1769 \pm 10 \text{ cm}^{-1}$ .

We note that this bond energy is unexpectedly high in comparison to other van der Waals dimers. The only other pair of HF rotational levels that gives a rotational energy difference within  $100 \text{ cm}^{-1}$  of the measured  $\Delta E_{\text{available}}$  has values of  $J_0 = 12$  and  $J_1 = 8$ , with an energy difference of  $1687 \text{ cm}^{-1}$ . This is  $2\sigma$  away from the best-fit value of  $1708 \text{ cm}^{-1}$ . The dashed lines drawn in Figs. 3(A) and 3(B) correspond to the best fit for the energetics consistent with this set of HF fragment states (slope of  $-1$  and  $1687 \text{ cm}^{-1}$

offset). As above, to fit the data within this scenario, and to satisfy conservation of energy constraints requires the presence of systematic errors in the determined recoil energies, here of about  $12 \text{ cm}^{-1}$ . The bond energy for this alternative pair of HF fragment states is  $448 \pm 5 \text{ cm}^{-1}$ .

Based on our recoil energy and product-state measurements, we cannot say which candidate bond energy,  $1770$  or  $450 \text{ cm}^{-1}$ , is correct since both values are within the range of conceivable ( $2\sigma$ ) uncertainty. Although the high value is in slightly better agreement with our data and is attractive because it pairs high- $J_{\text{HF}}$  fragments with principally high- $J_{\text{NO}(v=0)}$  fragments and low- $J_{\text{HF}}$  with low- $J_{\text{NO}(v=1)}$ , it exceeds the bond energies of both the strong hydrogen bond of the HF dimer ( $D_0 = 1065 \text{ cm}^{-1}$ ),<sup>6</sup> and the nearly covalent bond of the NO dimer ( $D_0 = 710 \text{ cm}^{-1}$ ).<sup>11</sup> The strong interactions in the pure dimers are not available to the mixed dimer; therefore, each of the homodimers is expected to be more strongly bound than the mixed dimer. A second objection to the higher  $D_0$  value is the following, intuitive argument. If  $D_0$  were ca.  $1770 \text{ cm}^{-1}$ , then fragment pairs HF( $J=2$ ) +  ${}^2\Pi_{1/2}$  NO( $v=1, J \leq 6.5$ ) are energetically open, as discussed above. Since the difference in rotational energies between HF( $J=2$ ) and HF( $J=1$ ) is relatively small, fragment pairs HF( $J=1$ ) +  ${}^2\Pi_{1/2}$  NO( $v=1, J \leq 9.5$ ) and, more importantly HF( $J=1$ ) +  ${}^2\Pi_{3/2}$  NO( $v=1, J \leq 5.5$ ) are also energetically open. This results in dissociation channels leading to two different HF( $J_i$ ) levels that are essentially degenerate in terms of linear and angular momentum release. None of the Doppler profiles observed for  ${}^2\Pi_{1/2}$  NO( $v=1, J \leq 6.5$ ) allow for HF( $J_i$ ) cofragments in more than a single rotational level, even for rotational levels as close in energy as HF( $J=1$ ) and HF( $J=2$ ). Early survey experiments, in which the signal-to-background levels obtained probing the  ${}^2\Pi_{1/2}$  NO( $v=1, J=3.5$ ) level were 10 to 20 failed to observe any significant population in any of the following levels:  ${}^2\Pi_{1/2}$  NO( $v=1, J=7.5, 8.5, \text{ or } 10.5$ ) or  ${}^2\Pi_{3/2}$  NO( $v=1, J=3.5, 4.5, \text{ or } 6.5$ ). The equal probability for populating both spin-orbit states in the HF( $J_0$ ) + NO( $v=0$ ) channel implies that spin-orbit selectivity is not the reason for the failure to observe population in  ${}^2\Pi_{3/2}$  NO( $v=1, J$ ) levels. Later, high signal-to-noise experiments showed a sharp decline in population in NO( $v=1, J$ ) levels around  $E_{\text{internal}}^{\text{NO}} \approx 1970 \text{ cm}^{-1}$  with a large population in the  ${}^2\Pi_{1/2}$  NO( $v=1, J=6.5$ ) level and no significant population in the next-higher energy  ${}^2\Pi_{1/2}$  NO( $v=1, J=7.5$ ) level. It is unlikely that the dissociation dynamics would so selectively discriminate against HF( $J=1$ ) dissociation channels in favor of HF( $J=2$ ) channels with so similar momentum gaps. Considering the lower value of  $D_0 = 450 \text{ cm}^{-1}$ , the momentum gaps associated with possible alternate HF( $J$ ) channels are much larger, by  $400$ – $500 \text{ cm}^{-1}$ . This should have the effect of restricting the dissociation to proceed through selective HF( $J_{0,1}$ ) channels as observed. Additional, indirect evidence that NO·HF is not anomalously strongly bonded comes from comparison of the  $\Delta\nu = -84 \text{ cm}^{-1}$  monomer to cluster H–F frequency shift in NO·HF to values<sup>1,5,6</sup> for OC·HF ( $\Delta\nu = -117 \text{ cm}^{-1}$ ;

$D_0 \approx 1000 \text{ cm}^{-1}$ ) and NN·HF ( $\Delta v = -43 \text{ cm}^{-1}$ ;  $D_0 \approx 600 \text{ cm}^{-1}$ ), and the fact that the dimer centers-of-mass separation determined by Fawzy *et al.* for NO·HF (3.4 Å) significantly exceeds the values for NO·NO (2.45 Å) and HF·HF (2.8 Å). Recoil momentum experiments, such as performed for HF·HF by Dayton, Jucks, and Miller,<sup>6</sup> with double-resonance detection to identify one of the fragment HF species, would conclusively prove the correct bond energy.

#### IV. SUMMARY

Following the excitation of NO·HF( $v=1, J=4.5-6.5$ ), two dissociation channels proceed with similar probability to produce NO( $v=0$ ) and NO( $v=1$ ). Most of the available energy appears in NO vibration and/or HF rotation with only a small amount of energy available for NO rotation. Each NO( $v, J$ ) fragment is formed with  $\delta$ -function recoil kinetic-energy distributions in concert with HF fragments in a single rotational level. Only two rotational levels of HF are populated,  $J_0$  and  $J_1$ , with HF( $J_0$ ) and HF( $J_1$ ) fragments paired exclusively with NO( $v=0$ ) and NO( $v=1$ ) fragments, respectively. There is little recoil momentum generated. For the channel resulting in NO( $v=1, J=6.5$ ) + HF( $J_1$ ), the recoil energy is only about  $15 \text{ cm}^{-1}$ . This gives an exit speed to the NO fragments of only 44 m/s. The presence of significant amounts of vibrationally excited NO fragments, in the absence of observable spectroscopic perturbations, implies that intramolecular vibrational redistribution proceeds as the dimer dissociates.

The observed rotational-population distributions for NO( $v=0$ ) fragments in both spin-orbit states have maxima just below the energetic cutoff ( $272 \text{ cm}^{-1}$ ). All energetically accessible levels observed are otherwise populated with similar probability. This is consistent with linear momentum-gap expectations, favoring populations in near-resonant exit channels. The NO( $v=1$ )-fragment rotational-population distributions, however, for which the maximum recoil energy ( $95 \text{ cm}^{-1}$ ) is significantly lower, are fairly flat up to the energetic cutoff. This result implies that constraints on fragment angular momenta as well as energetics are important for the dissociation dynamics of this reaction channel. Although a value of  $D_0 = 448 \pm 5 \text{ cm}^{-1}$  is preferred for the NO·HF dimer bond energy, this point is still open to

debate and has strong implications for the important bonding interactions in this complex.

- <sup>1</sup> R. E. Miller, *Acc. Chem. Res.* **23**, 10 (1990).
- <sup>2</sup> K. C. Janda, *Adv. Chem. Phys.* **60**, 201 (1985).
- <sup>3</sup> D. J. Nesbitt, *Chem. Rev.* **88**, 843 (1988).
- <sup>4</sup> M. P. Casassa, *Chem. Rev.* **88**, 815 (1988).
- <sup>5</sup> M. A. Benzel and C. E. Dykstra, *J. Chem. Phys.* **78**, 4052 (1983).
- <sup>6</sup> D. C. Dayton, K. W. Jucks, and R. E. Miller, *J. Chem. Phys.* **90**, 2631 (1989).
- <sup>7</sup> A. S. Pine, W. J. Lafferty, and B. J. Howard, *J. Chem. Phys.* **81**, 2939 (1984).
- <sup>8</sup> M. T. Berry, M. R. Brustein, J. R. Adamo, and M. I. Lester, *J. Phys. Chem.* **92**, 5551 (1988); M. T. Berry, M. R. Brustein, and M. I. Lester, *Chem. Phys. Lett.* **153**, 17 (1988); K. M. Beck, M. T. Berry, M. R. Brustein, and M. I. Lester, *ibid.* **162**, 203 (1989).
- <sup>9</sup> W. M. Fawzy and M. C. Heaven, *J. Chem. Phys.* **89**, 7030 (1988); **92**, 909 (1990).
- <sup>10</sup> D. S. King and J. C. Stephenson, *J. Chem. Phys.* **82**, 5286 (1985); M. P. Casassa, J. C. Stephenson, and D. S. King, *ibid.* **85**, 2333 (1986); M. P. Casassa, J. C. Stephenson, and D. S. King, *Faraday Discuss. Chem. Soc.* **82**, 251 (1986); M. P. Casassa, A. M. Woodward, J. C. Stephenson, and D. S. King, *J. Chem. Phys.* **85**, 6235 (1986); M. P. Casassa, J. C. Stephenson, and D. S. King, *ibid.* **89**, 1966 (1988).
- <sup>11</sup> J. R. Hetzler, M. P. Casassa, and D. S. King, *J. Phys. Chem.* **95**, 8086 (1991).
- <sup>12</sup> Ph. Brechignac, S. DeBenedicts, N. Halberstadt, B. J. Whitaker, and S. Avriillier, *J. Chem. Phys.* **83**, 2064 (1985); Y. Matsumoto, Y. Oshima, and T. Michio, *ibid.* **92**, 937 (1990).
- <sup>13</sup> K. J. Rensberger, J. T. Blair, F. Weinhold, and F. F. Crim, *J. Chem. Phys.* **91**, 1688 (1989).
- <sup>14</sup> W. M. Fawzy, G. T. Fraser, J. T. Hougen, and A. S. Pine, *J. Chem. Phys.* **95**, 7086 (1991).
- <sup>15</sup> R. A. Baumgartner and R. L. Byer, *IEEE J. Quantum Electron.* **QE-15**, 432 (1979).
- <sup>16</sup> M. P. Casassa, B. R. Foy, J. C. Stephenson, and D. S. King, *J. Chem. Phys.* **94**, 250 (1991).
- <sup>17</sup> D. M. Gates, R. F. Calfee, D. W. Hansen, and W. S. Benedict, *Natl. Bur. Stand. (U.S.) Monogr.* **71** (1964).
- <sup>18</sup> Band contours were calculated for us by A. S. Pine using the spectroscopic constants of Ref. 14 and neglecting contributions from dimer levels with  $K \neq 0$ .
- <sup>19</sup> R. N. Dixon, *J. Chem. Phys.* **85**, 1866 (1986).
- <sup>20</sup> K.-H. Gericke, S. Klee, F. J. Comes, and R. N. Dixon, *J. Chem. Phys.* **85**, 4463 (1986).
- <sup>21</sup> R. Engleman, Jr., P. E. Rouse, H. M. Peek, and V. D. Baiamonte, Los Alamos Scientific Laboratory, Report LA-4364, 1969.
- <sup>22</sup> C. M. Lovejoy and D. J. Nesbitt, *J. Chem. Phys.* **90**, 4671 (1989).
- <sup>23</sup> D. C. Dayton, P. A. Block, and R. E. Miller, *J. Phys. Chem.* **95**, 2881 (1991).
- <sup>24</sup> C. M. Lovejoy, D. D. Nelson, and D. J. Nesbitt, *J. Chem. Phys.* **87**, 5621 (1987); **89**, 7180 (1988).
- <sup>25</sup> D. C. Clary, *J. Chem. Phys.* **96**, 90 (1992).
- <sup>26</sup> G. E. Ewing, *J. Chem. Phys.* **90**, 1790 (1986).
- <sup>27</sup> H. G. Hedderich, K. Walker, and P. F. Bernath, *J. Mol. Spectrosc.* **149**, 314 (1991).